Construction and Building Materials 163 (2018) 622–633

Contents lists available at ScienceDirect

Construction and Building Materials

journal homepage: www.elsevier.com/locate/conbuildmat

Numerical study on notched steel beams strengthened by CFRP plates

Jun Deng, Junhui Li, Yi Wang *, Weizhi Xie

School of Civil and Transportation Engineering, Guangdong University of Technology, Guangzhou 510006, China

HIGHLIGHTS

- Mixed-mode cohesive law was employed in simulation of notched steel beams strengthened by CFRP plate.
- Crack propagation and CFRP plate debonding processes were well simulated.
- Plastic behaviour of the CFRP strengthened notched steel beams was revealed.

ARTICLE INFO

Article history:
Received 13 October 2017
Received in revised form 3 December 2017
Accepted 13 December 2017

Keywords:
Stress analysis
CFRP
Steel beams
Notch
Debonding
Numerical analysis

ABSTRACT

Carbon fibre reinforced polymer (CFRP) externally bonding is an efficient and effective method to strengthen damaged steel beams, and thereby prolong their service life. However, debonding failure, which requires accurate predictions to ensure safety, can occur before the full usage of CFRP. In this study, the notched steel beams strengthened with CFRP plate were simulated by finite element method where the mixed-mode cohesive law was employed to determine the interfacial stress. The load–deflection curves and strain development at different load levels from experimental study were used to verify the validity of the numerical model. The interfacial stress distribution with increasing load was analysed, and good correlation with theoretical calculations at elastic stage was observed. In contrast to the previous elastic analytical study, the plastic behaviour of the CFRP strengthened notched steel beams was revealed. More importantly, interfacial crack initiation, propagation and debonding were accurately simulated. This simulation method can be used to predict debonding process in actual engineering applications. In addition, parametric analysis was conducted to assess the effects of notch depth, CFRP elastic modulus and CFRP thickness. The ultimate load and ductility decreased substantially with increasing notch depth. Furthermore, although increased bearing capacity was achieved by increasing the CFRP elastic modulus and thickness, ductility decreased and premature debonding failure occurred more easily.

1. Introduction

The use of fibre reinforced polymer (FRP) to strengthen concrete structures has been extensively studied in recent decades [8,11,21,53,54,55], while carbon fibre reinforced polymer (CFRP) is favoured for strengthening steel structures due to its higher stiffness [22,26,34,35,38,40,52]. The load capacity and stiffness of steel structures, as well as the fatigue life, can be improved by externally bonded with CFRP [14,27,39,49]. However, prior to the full usage of CFRP, premature debonding failure may occur [3,15,17,28,30,32,33], which limits the wide application of the strengthening technique. To clarify the debonding mechanism, researchers have studied the bond behaviour of the CFRP/steel interface [2,10,13,20,36,42,44,45,50]. The common debonding failure modes are cohesive failure (delamination of CFRP or adhesive) and adhesive failure (debonding between the adhesive layer and steel) [52]. Single lap [50] and double strap [18,19] shear tests were conducted to determine the bond-slip relationship, which is important for understanding of the adhesive debonding failure. While delamination failure was considered to occur mainly due to the shear stress concentration, the normal stress concentration is also an important factor [7,9,37,41]. Therefore, both of the slip and separation result in debonding failure, it is necessary to study the bond behaviour of CFRP and steel beams with consideration of the two effects. The mixed-mode cohesive law was applied to simulate the debonding failure of continuous steel beams strengthened by CFRP plates with consideration of both the shear and normal stress concentrations [6,41]. However, strengthened steel beams usually have defects and have different failure modes compared with the case of sound steel beams [15,16,25,56]. The mechanical performance of notched steel beams strengthened by CFRP plates requires further investigation.

* Corresponding author.
E-mail addresses: jdeng@gdut.edu.cn (J. Deng), wangyi@gdut.edu.cn (Y. Wang).

https://doi.org/10.1016/j.conbuildmat.2017.12.110
0950-0618/

There are two main theoretical methods to predict the mechanical performance of steel structures strengthened by FRP: fracture mechanics and stress-based criteria [3]. For the latter, researchers have focused on steel plates and steel beams [24,48]; however, the theoretical analysis is limited to elastic stage, for which the stress concentration is overestimated [4,41]. Theoretical and experimental studies have also been conducted on notched steel beams [15]. The results basically agree in the elastic stage, but difference becomes obvious in the plastic stage. The actual debonding process cannot be predicted accurately. The theoretical result can be useful in simplifying the design, but it is inadequate for the mechanical performance evaluation. In contrast, fracture mechanics is considered as a more reliable debonding prediction method [29]. Numerical studies can be conducted based on the fracture mechanics. It could be a common useful method for debonding prediction because only typical cases have been considered in experimental study and the results are difficult to apply in practice [23,31,47,51].

In this study, the mixed-mode cohesive law was applied to simulate the stress distribution and debonding process of notched steel beams strengthened by CFRP plates. Previous theoretical and experimental results [15] were used to verify the numerical results. The purpose was to develop a numerical method to simulate the debonding failure of CFRP strengthened notched steel beams with consideration of plastic behaviour and to provide useful information for debonding prevention by parameter analysis.

2. Theoretical background

The most common failure mode of strengthened steel structures is debonding. As shown in Fig. 1, there are three types of fracture modes. Mode I, opening, usually occurs in the delamination of CFRP and cohesive failure of the adhesive layer. The fracture is due to the normal stress concentration. Mode II, shear cracking, is due to the shear stress concentration. Mode III, tearing cracking, is a mixture of Mode I and Mode II. The constitutive laws have been developed for Mode I, Mode II and Mode III (bond-separation model and bond-slip model for both shear directions), as shown in Fig. 2(a) and (b), respectively. According to the mixed-mode of interface debonding, both of the shear and normal stresses concentration were considered. For accurate prediction of debonding, the mixed-mode cohesive law was proposed for numerical simulation [41,43], in which pure Mode I, Mode II and Mode III can be simulated. The details of each model are described below.

2.1. Bond-separation model

The bi-linear bond-separation model followed the approach suggested by Camanho et al. [6] and Campilho et al. [7], as shown in Fig. 2(a). When the adhesive layer is damaged by pure tension, the damage of the adhesive layer initiates when the normal stress exceeds its tensile strength (f_t), which can be obtained from material test results. With increasing of crack opening, the normal traction stress (t_n) decreases gradually until reaching zero, and the corresponding displacement is defined as the final failure displacement (δ_n^f).

$$t_n = \begin{cases} K_n\delta_n & \text{if } \delta_n \leqslant \delta_n^0 \\ K_n\delta_n(1-d_n) & \text{if } \delta_n^0 < \delta_n \leqslant \delta_n^f \\ 0 & \text{if } \delta_n > \delta_n^f \end{cases}, \tag{1}$$

in which

$$K_n = \frac{E_a}{t_a};\ \delta_n^0 = \frac{f_t t_a}{E_a} \text{ and } d_n = \frac{\delta_n^f(\delta_n - \delta_n^0)}{\delta_n(\delta_n^f - \delta_n^0)}, \tag{2}$$

where K_i is the initial stiffness before cracking, δ_i is the opening displacement, δ_i^0 is the opening displacement at the point of initial interfacial cracking, δ_i^f is the final failure opening displacement when the normal traction force is zero, d_i is the damage factor due to the opening cracking (in the range of 0–1) ($i = n,s$, means normal and shear directions respectively), E_a is the elastic modulus of the adhesive layer, t_a is the thickness of the adhesive layer and f_t is the tensile strength of the adhesive layer.

Based on double cantilever beam tests, the final failure displacement can also be determined based on the interfacial fracture energy. The relationship was proposed by [1],

$$G_I = \frac{1}{2} f_t \delta_n^f, \tag{3}$$

where G_I is the interfacial fracture energy of Mode I failure.

2.2. Bond-slip model

Xia and Teng [46] proposed an interfacial bond-slip model to predict the bond behaviour of the steel-FRP interface, as shown in Fig. 2(b). Similar to the bond-separation model, it is also a bi-linear relationship. We define the adhesive shear strength (τ_s) as the interfacial debonding strength, and it can be determined by the tensile strength of the adhesive layer ($0.8f_t$). The relationship of the shear traction stress (t_s) and slip displacement (δ_s) can be defined as

$$t_s = \begin{cases} K_s\delta_s & \text{if } \delta_s \leqslant \delta_s^0 \\ K_s\delta_s(1-d_s) & \text{if } \delta_s^0 < \delta_s \leqslant \delta_s^f \\ 0 & \text{if } \delta_s > \delta_s^f \end{cases}, \tag{4}$$

in which

$$K_s = \frac{G_a}{t_a};\ \delta_s^0 = \frac{f_t t_a}{G_a};\ \delta_s^f = \frac{2G_{II}}{\tau_s} = 62\left(\frac{f_t}{G_a}\right)^{0.56}\frac{t_a^{0.27}}{\tau_s} \text{ and } d_s = \frac{\delta_s^f(\delta_s - \delta_s^0)}{\delta_s(\delta_s^f - \delta_s^0)}, \tag{5}$$

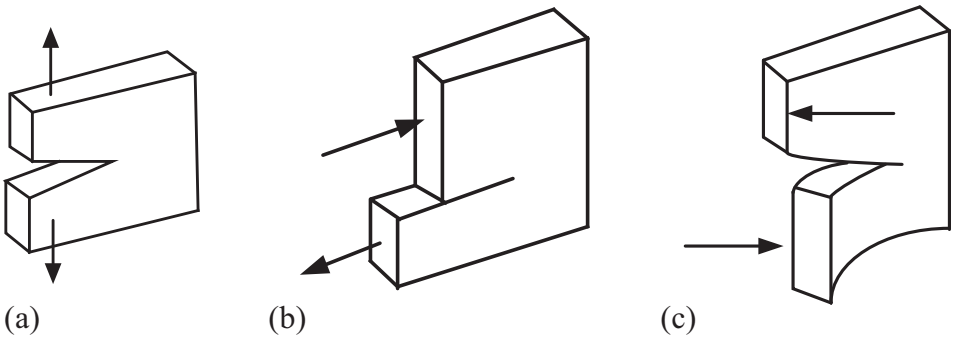

Fig. 1. Crack types: (a) Mode I; (b) Mode II; (c) Mode III.

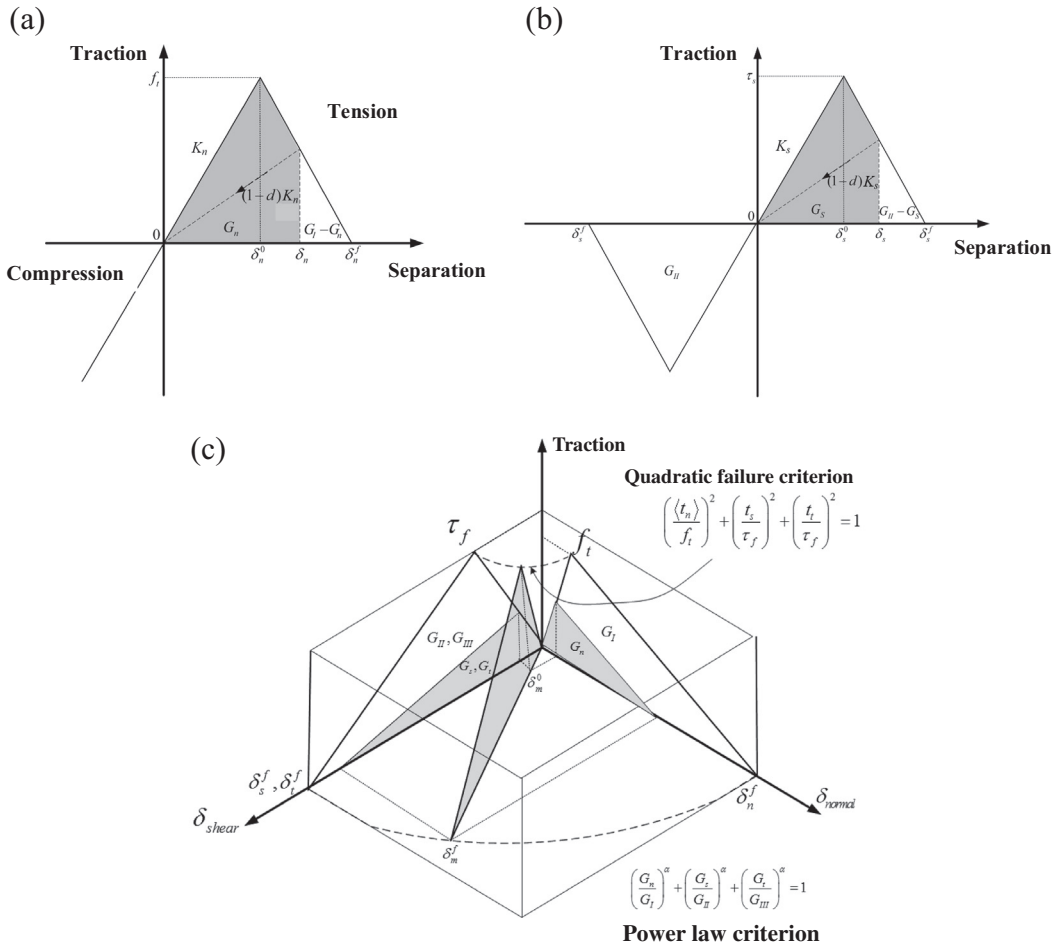

Fig. 2. Constitutive laws: (a) bond-separation model; (b) bond-slip model; (c) mixed-mode cohesive law.

where τ_s is the shear strength of adhesive layer, G_a is the shear modulus of the adhesive layer and G_{II} is the interfacial shear fracture energy per unit area. G_{II} can be calculated by the following equation

$$G_{II} = 31\left(\frac{f_t}{G_a}\right)^{0.56} t_a^{0.27}. \tag{6}$$

2.3. Mixed-mode cohesive law

According to the simultaneity of the three fracture modes, Camanho et al. [6] applied a mixed-mode cohesive law for finite element analysis, and the debonding process of composite materials was accurately simulated. Meanwhile, Teng et al. [41] also used the mixed-mode cohesive law to simulate sound steel beams strengthened by CFRP. The model considered the three fracture modes, which means that it was a combination of bond separation in the normal direction and bond slip in the two shear directions (see Fig. 2(c)). In this case, t_n, t_s and t_t represent the normal stress and shear stresses in two directions, and the corresponding displacements are δ_n, δ_s, and δ_t. If the initial thickness of the adhesive layer cohesive element is T_0 (it has the meaning of three directions which is different from t_a (normal direction)), the interfacial strains are

$$\varepsilon_n = \frac{\delta_n}{T_0}, \varepsilon_s = \frac{\delta_s}{T_0} \text{ and } \varepsilon_t = \frac{\delta_t}{T_0}. \tag{7}$$

In the elastic stage, the relationships between the traction stresses and displacements are

$$\begin{cases} t_n = K_n\delta_n \\ t_s = K_s\delta_s \\ t_t = K_t\delta_t \end{cases} \tag{8}$$

$$K_n = \frac{E_a}{T_0};\ K_s = K_t = \frac{G_a}{T_0}, \tag{9}$$

where K_n, K_s and K_t are the normal and two shear directions' initial stiffness.

In the damage evolution stage, the initiation of interfacial cracking can be determined by the quadratic failure criterion

$$\left(\frac{\langle t_n\rangle}{f_t}\right)^2 + \left(\frac{t_s}{\tau_f}\right)^2 + \left(\frac{t_t}{\tau_f}\right)^2 = 1, \tag{10}$$

where $\langle\rangle$ is the Macaulay bracket. $\langle t_n\rangle$ is zero when the normal stress t_n is negative. The physical meaning is that bond-separation failure will not occur if the adhesive layer is under compression.

To describe the interfacial damage evolution of both the normal and shear directions, an effective displacement δ_m is included [6] and can be calculated as

$$\delta_m = \sqrt{\langle\delta_n\rangle^2 + \delta_s^2 + \delta_t^2}, \tag{11}$$

where $\langle\delta_n\rangle$ is the opening displacement of the adhesive layer under tension.

Then, the damage factor can be reproduced as

$$d = \frac{\delta_m^f(\delta_m - \delta_m^0)}{\delta_m(\delta_m^f - \delta_m^0)}, \tag{12}$$

where $\delta_m{}^0$ is the effective displacement at the point of initial interfacial cracking, δ_m^f is the final failure effective displacement when the traction force is zero.

The mixed-mode fracture criterion can apply the power law, as provided by ABAQUS. The equation is then

$$\left(\frac{G_n}{G_I}\right)^{\alpha}+\left(\frac{G_s}{G_{II}}\right)^{\alpha}+\left(\frac{G_t}{G_{III}}\right)^{\alpha}=1, \tag{13}$$

where G_I, G_{II} and G_{III} are the interfacial fracture energies of the three directions, respectively. Parameter α is taken as 1 for simplicity. In this case, it becomes a linear fracture criterion.

3. Summary of test programs

As presented in our previous study, notched steel beams strengthened by CFRP plates were prepared for four-point bending test [15]. The geometry of the specimens is shown in Fig. 3. The steel had a yield strength of 305.3 MPa, a tensile strength of 460 MPa and a Young's modulus of 205.1 GPa, whereas the CFRP plate had a tensile strength of 745.9 MPa, Poison's ratio of 0.3 and a Young's modulus of 127.2 GPa in the fibre direction. In addition, Sikadur-30 adhesives for bonding steel were employed in the test. According to the manufacture's instruction, the adhesive has a tensile strength of 25.5 MPa, a shear strength of 18 MPa, a shear modulus of 4.3 GPa and a Young's modulus of 11.2 GPa. The ultimate tensile strain is 0.0035. The thickness of the adhesive layer was approximately 1 mm. Four-point bending tests were conducted, and the debonding load, ultimate load, strain and corresponding deflections were obtained. For CFRP strengthened steel beams, the strain distribution was measured by 2 mm long strain gauges

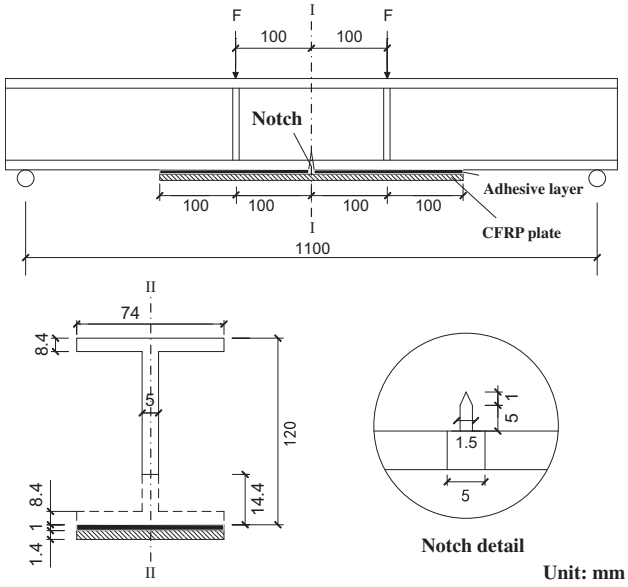

Fig. 3. Details of the strengthened steel beam.

along the longitudinal centre line of CFRP plate (nine strain gauges mounted on the bottom of CFRP plate, four on the steel beam flanges and one on the web in the mid-span of specimen). For notched steel beams without strengthening, one strain gauge was mounted at the notch tip. Besides, a potentiometer was placed in the middle of the specimens to measure the deflections. A camera was used to monitor the debonding progress near the position of the notch. Details of the test results [15] are shown in Table 1.

4. FE model

According to our previous experimental study [15], a finite element (FE) model (notched steel beam-adhesive layer-CFRP plate) was developed and verified by the experimental results. The geometry and material properties of the specimen in Section 3 were applied in this model. According to the adhesive properties, the displacement at debonding load and the interfacial fracture energy in the normal direction (Mode I) were obtained based on the theory discussed in Section 2, whereas the two shear directions applied the parameters as same as in Mode II. The key parameters for the traction-separation model are shown in Table 2.

For the notched steel beam and CFRP plate, the eight-node three-dimensional non-coordinative solid element (C3D8I) was used for the simulation. The element was chosen due to its accuracy in simulating the problems of bending and contact. The adhesive layer plays an essential role in stress transfer between the steel beam and the CFRP plate, so it is the key point for the simulation model. The eight-node three-dimensional cohesive element (COH3D8) was applied in the mixed-mode bond degradation model. Because the cohesive element can consider the behaviour of materials in the thickness direction, it was developed in ABAQUS based on the traction-separation model, in which the interface is not the weak point. The accuracy of the cohesive element has been proved by many existing studies [5,41].

Adhesive layer damage evolution was applied to represent interface failure damage. Before debonding failure, the CFRP and steel beam were assumed to be compatible. As a result, the steel/adhesive and adhesive/CFRP interfaces used TIE for bonding and were meshed with the same size, which means that the interface of the two different materials had no freedom. The relationship of the adhesive principle stress at the notch and the number of elements when the load is 6.3 kN are shown in Fig. 4. The convergence of the FE model occurs when the adhesive element reaches 1200 as the principle stress remains constant. Considering the efficiency

Table 2
Parameters for the traction-separation models.

Bond model (mixed-mode)	Debonding strength (MPa)	Displacement at debonding load (mm)	Interfacial fracture energy (N/mm)
Normal stress (Mode I)	27	0.00241	0.0473
Shear stress (Mode II)	18	0.00418	1.81

Table 1
Details of the test results [15].

Specimen	Notch	Repair	Ultimate load (kN)	Deflection (mm)	Failure mode
C-1	Without	No	52.9	37.2	Steel buckling
A-1	With	No	21.5	4.6	Notch propagation
A-2	With	No	22.2	5.3	Notch propagation
AR-1	With	Yes	41.0	6.1	CFRP debonding
AR-2	With	Yes	40.9	5.2	CFRP debonding
AR-3	With	Yes	40.4	5.5	CFRP debonding

Note: The failure mode 'steel buckling' means the compressive up flange buckling.

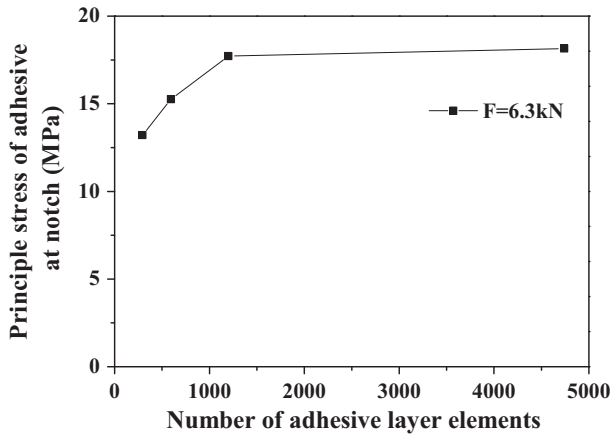

Fig. 4. Convergence of the finite element model.

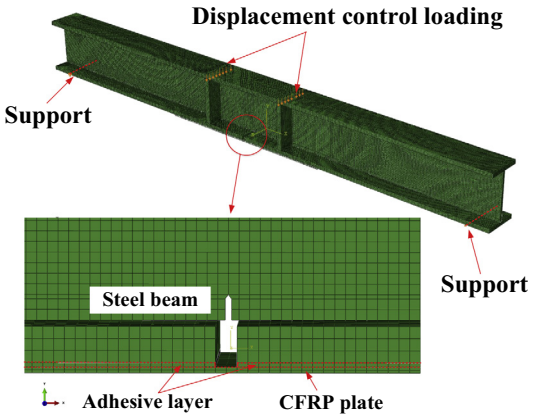

Fig. 5. Finite element model mesh.

and accuracy, the FE model meshing was conducted as below (see Fig. 5): adhesive mesh size (2.5 mm × 2.5 mm × 1 mm (1 mm is the thickness)), steel beam mesh size (2.5 mm × 2.5 mm × 2.5 mm) and CFRP plate mesh size (2.5 mm × 2.5 mm × 0.7 mm (0.7 mm is the CFRP thickness)).

5. Results and discussions

5.1. Load-deflection curves

As shown in Fig. 6, the simulated results agree with the experimental results for the notched steel beams and CFRP plate strengthened notched steel beams. The results validated the reasonability of the parameters selected in the FE model and the accuracy of the simulation model for notched steel beams strengthened with CFRP plate. The load-deflection curves of the notched steel beams and the CFRP plate strengthened notched steel beams are shown in Fig. 6(a) and (b), respectively. They all show plastic behaviour due to the plastic state of up flange and notched part of steel beam. The steel near the notch could be in plastic state at a rather low load level. It could have marginal influence on the plastic behaviour of steel beam. However, with load increases, the up flange of steel beam under compression could turn to the plastic state. Then the plastic behaviour of the notched steel beams becomes clear. For notched steel beam (see Fig. 6(a)), the up flange of steel beam turns to the plastic state soon after the yielding of steel near the notch. Then the notch propagation becomes the failure mode. While for CFRP strengthened notched steel beams (see Fig. 6(b)), the up flange of steel beam becomes plastic state when the load increased to more than 30kN. Because the CFRP externally bonding can reduce the stress concentration at the notch, the steel yield at the notch could be impeded, as well as the up flange steel yielding. When the CFRP strengthened steel beam show obvious plastic behaviour, the notch of the steel beam starts to propagate before the debonding initiated. After the debonding of CFRP plate, the notch crack propagation is accelerated and becomes failure finally. The ultimate load and ductility were largely improved after strengthening. It is worthy to note that the loads of strengthened specimens after debonding were similar to those in the cases without strengthening.

5.2. Longitudinal strain distribution in CFRP plates

The bond behaviour is important for the overall mechanical performance of the composite strengthening system, especially for understanding of the debonding failure. While the failure mode of steel beams without notches is usually CFRP plate-end debonding, it becomes intermediate debonding when the steel beam has a notch because of the stress concentration at the notch [13,15]. For CFRP strengthened steel beams with and without notches, the strains development with the CFRP bondline are also different. Therefore, the strains distribution along the CFRP plate at debonding load and ultimate load were simulated and compared with the test results, as shown in Fig. 7. It is clear that the results showed good agreement. The figure shows that the debonding failure occurs near the notch (Fig. 7 a) and then propagated toward the plate ends (Fig. 7 b). For the specimen at debonding load, the strain reached its maximum at the notch, and the strain remained a low value at 100 mm away from the notch. When the load reached the ultimate load, the strain rapidly increased to the maximum from the CFRP plate end to the location 100 mm away from CFRP plate end. After that, up to the notch, the strains remained almost constant. It indicates that the stress concentration area propagates from the notch toward the CFRP plate end with load increase (from debonding load to ultimate load). The increased difference near the notch can be explained by the lower stiffness of the notched steel beam in the FE model, as shown in Fig. 6a. The results validated the reliability and accuracy of the FE model.

5.3. Load capacity of notch-damaged steel beams strengthened by CFRP plates

As shown in Table 3, the debonding load, ultimate load and deflection from the FE model were compared with the test results of notched steel beams strengthened by CFRP plates, and the deviation was calculated. The scattering of the test results was obvious, and the FEM results essentially agree, indicating that the FE simulation is applicable for predicting the debonding and ultimate loads and the maximum deflection.

5.4. Interfacial stress distribution

According to the simulation results, the longitudinal shear stress and normal stress distributions with the CFRP plate bondline are shown in Figs. 8 and 9 for different load levels. When the load level was 6.25 kN, the interfacial stress concentration initiated at positions close to the notch and CFRP plate ends. The maximum shear stress was near the notch and was much greater than that near the CFRP plate ends. As the load increased to 9.36 kN, the area of interfacial stress concentration near the notch increased, and the normal stress reached the maximum along the CFRP plate bondline. When the load reached 20.88 kN, the maximum shear stress shifted to a position 20 mm from the mid-span, indicating that the interfacial stress concentration moved from the notch towards

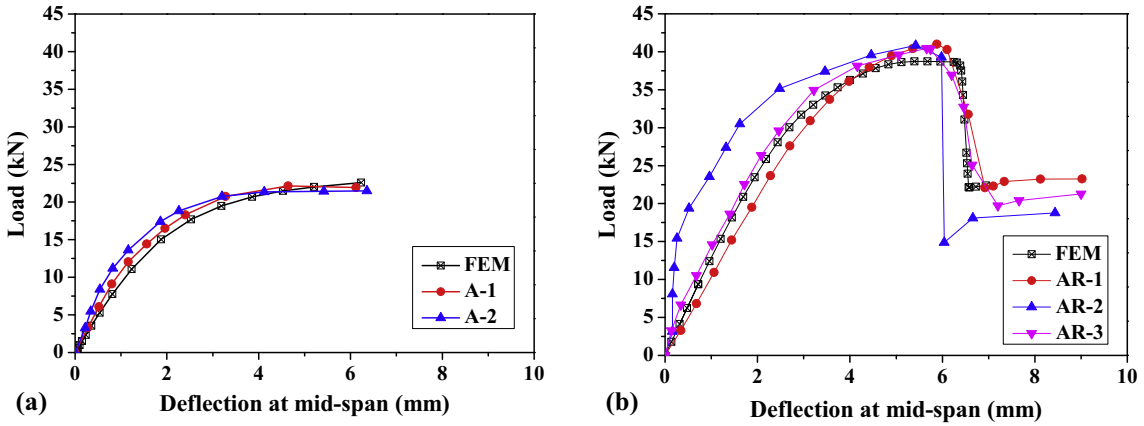

Fig. 6. Load-deflection curves of (a) notched beam (b) notched beam strengthened with CFRP plate.

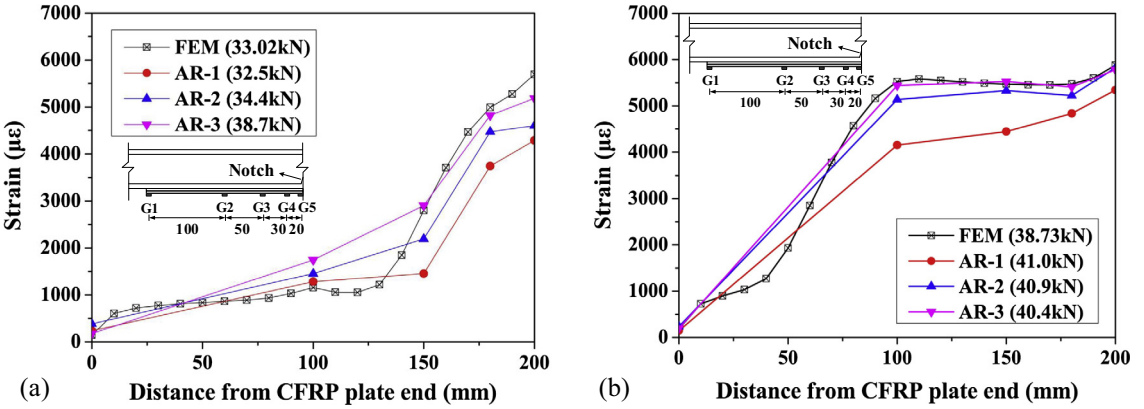

Fig. 7. Comparison of the experimental and finite element model strains at (a) debonding load (b) ultimate load.

Table 3
Capacity comparison of the experimental results and finite element model.

Steel beams	Debonding load (kN)	Deviation	Ultimate load (kN)	Deviation	Deflection in mid-span at ultimate load (mm)	Deviation
FEM	33.02	/	38.73	/	5.95	/
AR-1	32.5	−1.6%	41.0	5.5%	5.88	1.2%
AR-2	34.4	4.0%	40.9	5.3%	5.42	−9.8%
AR-3	38.7	14.7%	40.4	4.1%	5.66	−5.1%

the CFRP plate ends. In the FE model, after the interfacial stress exceeds the strength of the material, the element is invalid, and the interfacial stress becomes zero. Therefore, at a load of F = 33.02 kN (debonding load), the interfacial stress at position less than 5 mm away from the mid-span were zero, and the maximum shear stress moved to a position 60 mm away from the mid-span. Furthermore, when the load reached the ultimate load of 38.73 kN, the zero interfacial stress transferred to a position 90 mm from the mid-span and complete debonding of the CFRP was observed after a slight decrease in load.

According to the theoretical background, the initiation of debonding will not occur when the adhesive layer is under compression. As shown in Fig. 8, before debonding failure, the normal stress near the notch was always positive and remained small, whereas the shear stress was much higher and the maximum shifted from the notch to the CFRP plate ends. Therefore, the intermediate debonding failure was mainly due to the shear stress concentration near the notch.

With regard to the damage mode of the notched steel beam strengthened by CFRP plate, three composite specimens had similar test results. Specifically, beam AR-1 was in the elastic stage, and no cracking was observed when the load reached 32 kN. Based on the camera monitoring, initiation cracking was observed in the adhesive layer near the notch of the steel beam when the load was 32.5 kN. As the load increased, the interfacial crack propagated continuously. After the load reached the ultimate load 41.01 kN, the load decreased slowly, and deformation of the steel beam web was observed at the notch. As the load decreased to 40.2 kN, one side of the CFRP plate debonded completely, whereas a small part maintained bonding on the other side. However, as shown by the numerical model, the interfacial shear and normal stresses reached their maximum values at a load of 6.25 kN and then decreased, as observed in the case of a load equal to 9.36 kN. As the load increased to 20.88 kN, obvious softening of adhesive layer close to the notch was observed. Moreover, the adhesive element became invalid when the load reached the debonding load 33.02 kN because cracks could initiate, and the number of invalid elements increased with the load. The adhesive elements were entirely invalid at the notch when the load reached the ultimate load of 38.73 kN. Then, the load decreased slightly to 37.53 kN

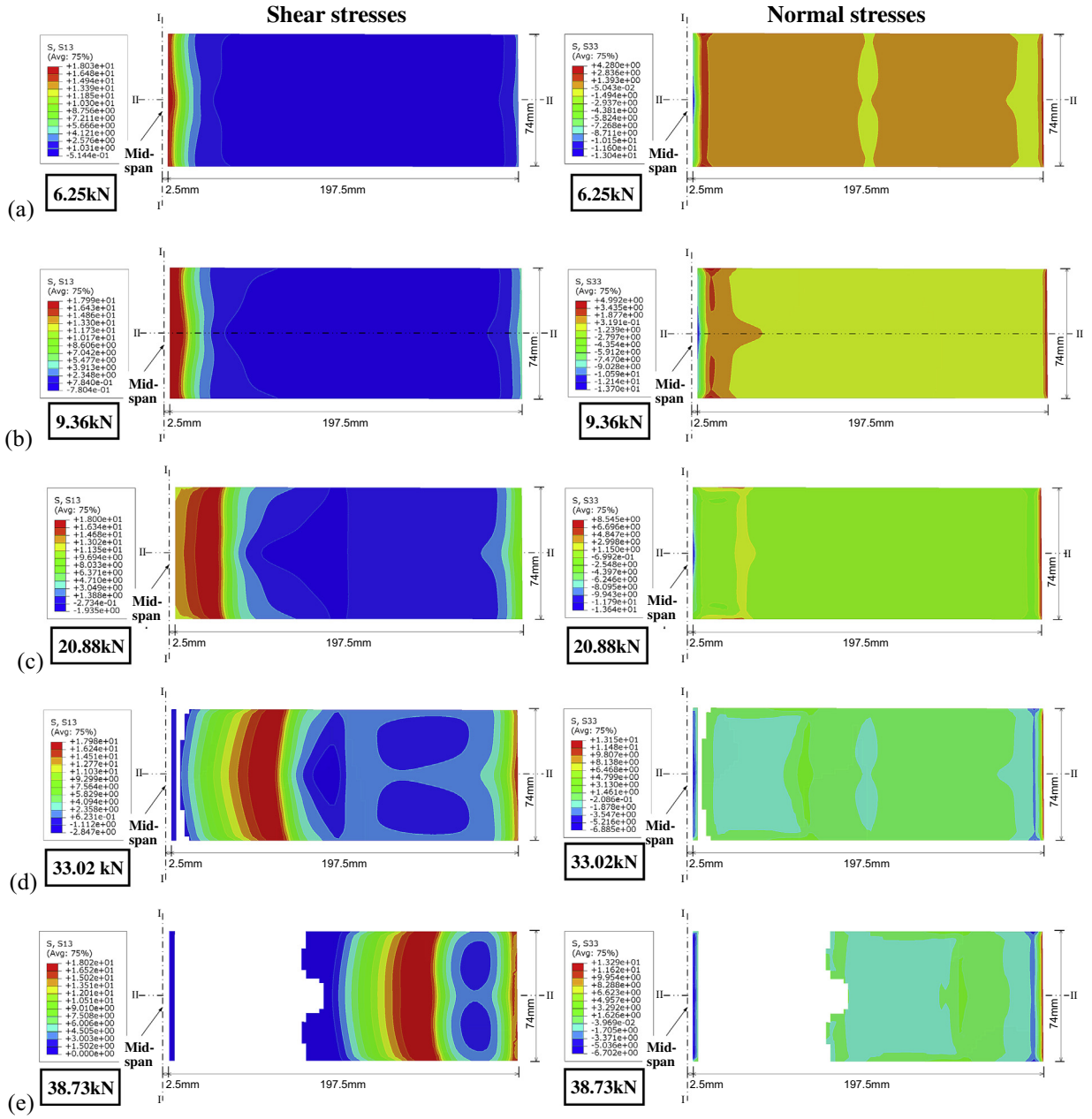

Fig. 8. Stresses in the adhesive according to the finite element model at load levels of (a) 6.25 kN (b) 9.36 kN (c) 20.88 kN (d) 33.02 kN (debonding load) and (e) 38.73 kN (ultimate load).

before dropping dramatically without a major change in deflection. Finally, CFRP debonding failure was observed, and all the adhesive elements on the right side of the beam became invalid. Therefore, the debonding process results from the test agree with the simulation results. The adhesive crack initiation starts at the notch and moves toward the CFRP plate end, resulting in debonding failure. These results further verified the applicability and reliability of the FE model.

5.5. Comparisons of the analytical and FEM interfacial stress distributions

Theoretical study on notched steel beams strengthened with CFRP plate was reported in our previous publication [15]. As derived, the equations for calculating of interfacial shear and normal stresses are summarized as below

$$\tau = -\frac{\lambda c}{b}e^{-\lambda x} + \frac{Z_s}{bf_2E_sI_s}(V_1(x) - V_p(x)) \tag{14}$$

$$\sigma(x) = e^{-\beta x}(s_1 cos(\beta x) + s_2 sin(\beta x)) + \frac{f_5}{f_4}\frac{d\tau}{dx} \tag{15}$$

in which

$$\lambda = \sqrt{\frac{f_2}{f_1}},\ \beta = \sqrt[4]{\frac{f_4}{4f_3}},\ f_1 = \frac{t_a}{Gb},\ f_2 = \frac{(Z_s + Z_f)Z_s}{E_sI_s} + \frac{1}{E_sA_s} + \frac{1}{E_fA_f},$$
$$f_3 = \frac{t_a}{E_ab},\ f_4 = \frac{1}{E_sI_s} + \frac{1}{E_fI_f},\ f_5 = \frac{Z_s}{E_sI_s} - \frac{Z_f}{E_fI_f} \tag{16}$$

where E, I, G and A are the elastic modulus, the second moment of area, rigidity modulus and the area. The subscripts s, f and a denote steel beam, CFRP plate and adhesive, c is a constant value. Z_s, Z_f, t_a

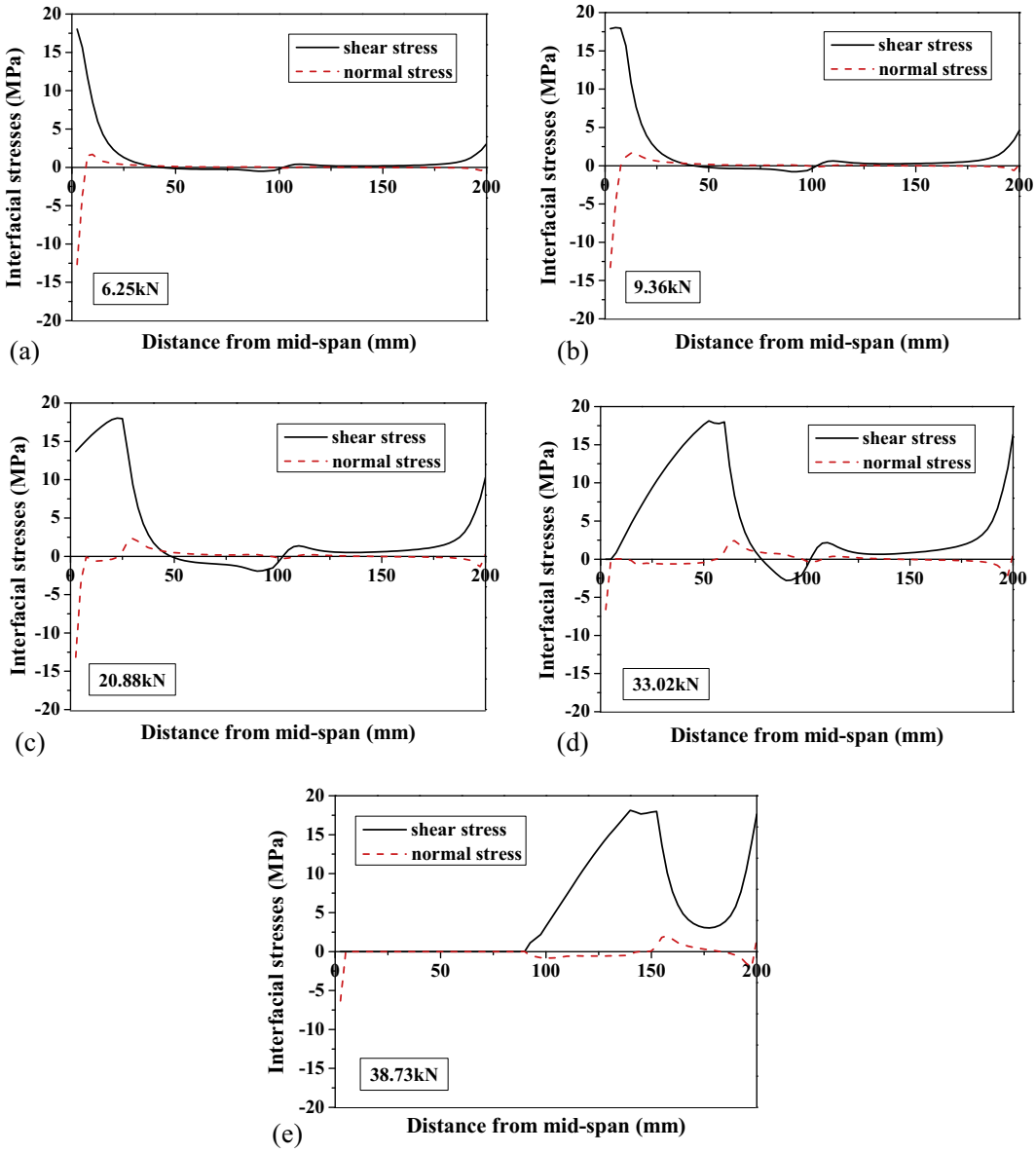

Fig. 9. Interfacial stress distributions along section II-II at load levels of (a) 6.25 kN (b) 9.36 kN (c) 20.88 kN (d) 33.02 kN (debonding load) and (e) 38.73 kN (ultimate load).

and b are the distance from the neutral axis to the bottom of the steel beam, the distance from the neutral axis to the top of the CFRP plate, the adhesive thickness and CFRP plate width. $V_1(x)$ and $V_p(x)$ are the shear forces caused by applied loading and load-relief jacking.

The boundary conditions are employed to obtain s_1 and s_2.

(1) CFRP plate ends

$$s_1 = \frac{c}{2\beta^3 b}\left(-\frac{f_5}{f_3}\lambda + \frac{f_5}{f_4}\lambda^5 - \beta\frac{f_5}{f_4}\lambda^4\right) + \frac{1}{2\beta^3}\left(\frac{f_5 Z_s}{f_3 b f_2 E_s I_s}V_1(0) - \frac{\beta E_a}{t_a}\frac{M_1(0)}{E_s I_s} - \frac{E_a}{t_a}\frac{V_1(0)}{E_s I_s}\right) \quad (17)$$

$$s_2 = \frac{1}{2\beta^2}\left(\frac{E_a}{t_a}\frac{M_1(0)}{E_s I_s} + \frac{f_5}{f_4}\frac{c}{b}\lambda^4\right) \quad (18)$$

where $M_1(0)$, $V_1(0)$ are the bending moment and shear force of the CFRP plate at the ends of the CFRP plate.

(2) Notch

$$s_1 = \frac{c}{2\beta^3 b}\left(-\frac{f_5}{f_3}\lambda + \frac{f_5}{f_4}\lambda^5 - \beta\frac{f_5}{f_4}\lambda^4\right) + \frac{1}{2\beta^3}\left(\frac{f_5 Z_s}{f_3 b f_2 E_s I_s}V_1(0) - \frac{\beta E_a}{t_a}\frac{M_1(0)}{(\overline{EI})_1} - \frac{E_a}{t_a}\frac{V_1(0)}{E_s I_s}\right) \quad (19)$$

$$s_2 = \frac{1}{2\beta^2}\left(\frac{E_a}{t_a}\frac{M_1(0)}{(\overline{EI})_1} + \frac{f_5}{f_4}\frac{c}{b}\lambda^4\right) \quad (20)$$

where $M_1(0)$, $V_1(0)$ are the bending moment and shear force of the CFRP plate at the notch location. $(\overline{EI})_1$ is the combined stiffness of the strengthened sections.

The interfacial stresses from the FE modelling and the analytical calculations for loads of 6.25 kN and 9.36 kN are shown in Fig. 10. Stress concentration appeared near the notch, and a good agreement was observed. When the load increased to 9.36 kN, the interfacial stress started to decrease in the FE modelling results, whereas no decrease was observed in the analytical results. The

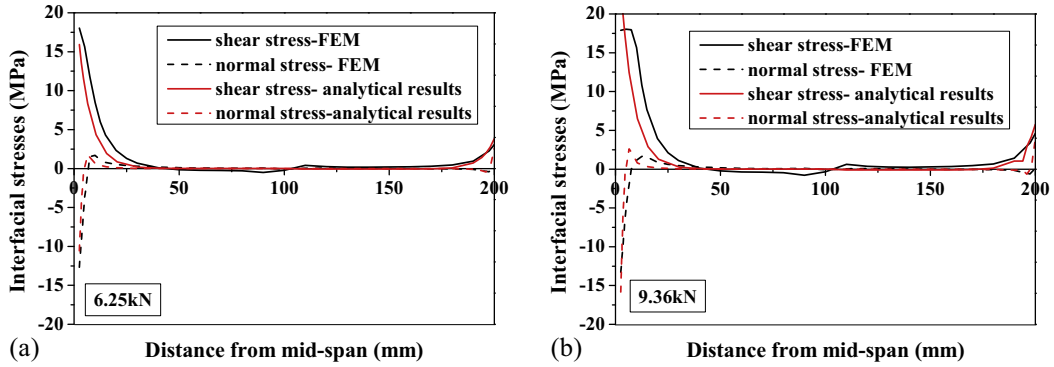

Fig. 10. Comparisons of the analytical and finite element model interfacial stress distributions along section II-II at load levels of (a) 6.25 kN and (b) 9.36 kN.

main reason for this difference is the simply elastic analysis used for the analytical calculations. The degradation process of the adhesive was not considered. Therefore, the analytical interfacial stress increased consistently and the debonding load was underestimated.

6. Parametric analysis

In this section, three parameters, notch depth, CFRP elastic modulus and thickness, were systematically analysed. Their influence on the bearing capacity and interfacial stress of notched steel beams strengthened by CFRP plates was discussed for a better understanding of the strengthening of damaged steel structures.

6.1. Notch depth

To understand the influence of the notch depth to the strengthening effect, three notch depths were modelled, 14.4 mm, 34.4 mm and 54.4 mm. The load-deflection at mid-span curve is presented in Fig. 11(a). The debonding and ultimate loads decreased with increasing notch depth, as did the deflection in accordance with the ultimate load. When the notch depth increased from 14.4 mm to 34.4 mm and 54.4 mm, the debonding load decreased 21.5% and 34.5%, the ultimate load decreased 18.6% and 34.6%, and the deflection decreased 7.3% and 12.2%, respectively. In addition, the interfacial stress developed with the load near the notch (where the adhesive was cracking), as shown in Fig. 11(b). At notch depths of 14.4 mm, 34.4 mm and 54.4 mm, the shear and normal stresses reached their maxima at loads of 9.36 kN, 5.99 kN and 5.81 kN and then reached zero at loads of 33.02 kN, 25.92 kN and 21.63 kN, respectively. The interfacial stress decreased after reaching the debonding load, which means adhesive layer softening initiated near the notch. Additionally, the deeper the notch was, the lower the load required for the initiation of adhesive layer degradation.

After the adhesive layer was softened, for deeper notches, the interfacial stress at the notch was lower and the decrease in stress was more rapid. As a result, the debonding load and ultimate load also decreased with increasing notch depth. Thus, deeper notches promoted cracking of the adhesive layer, which caused premature debonding failure by decreasing the bearing capacity and ductility. Therefore, CFRP strengthening should be designed with special considerations for deep-notched steel beams.

6.2. CFRP elastic modulus

Since steel beams have higher stiffness than concrete, the strengthening effect could be minimal if CFRP with a lower elastic modulus is applied. Some researchers have argued that better mechanical performance can be achieved if we use ultra-high elastic modulus CFRP [45]. To clarify the effect of the CFRP elastic modulus, three elastic moduli (127.2 GPa, 200 GPa and 250 GPa) were applied in the simulation, and the results are shown in Fig. 12. It is evident that the higher the elastic modulus is, the larger the ultimate load and debonding load that can be reached, although the deflection is lower (see Fig. 12(a)). When the CFRP elastic moduli increased from 127.2 GPa to 200 GPa and 250 GPa, the debonding load increased 15.1% and 26.4%, the ultimate load increased 11.4% and 17.8%, whereas the deflection decreased 8.3% and 9.4%, respectively. Thus, ultra-high elastic modulus CFRP is suitable for improving the bearing capacity of steel beams, but the reduction in ductility should be considered for premature debonding failure.

Accordingly, the interfacial stress changes with load was also analysed for steel beams strengthened with CFRP plates with dif-

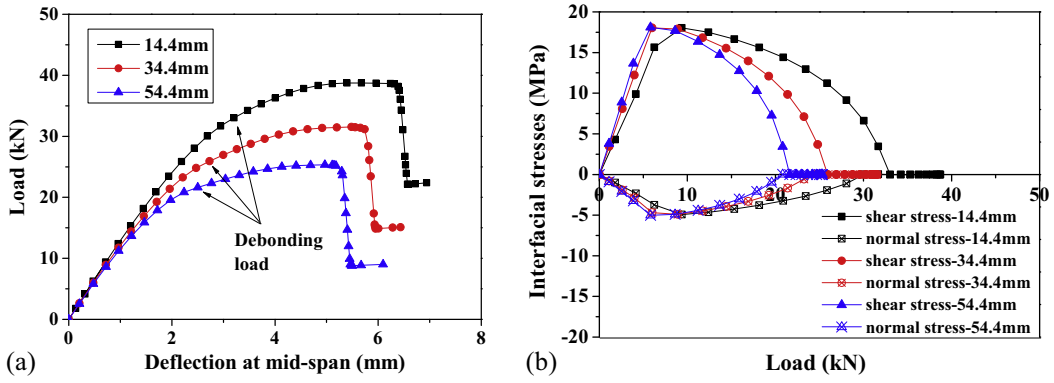

Fig. 11. Strengthened beam with different notch depths: (a) Load-deflection relationship; (b) Interfacial stress-load relationship.

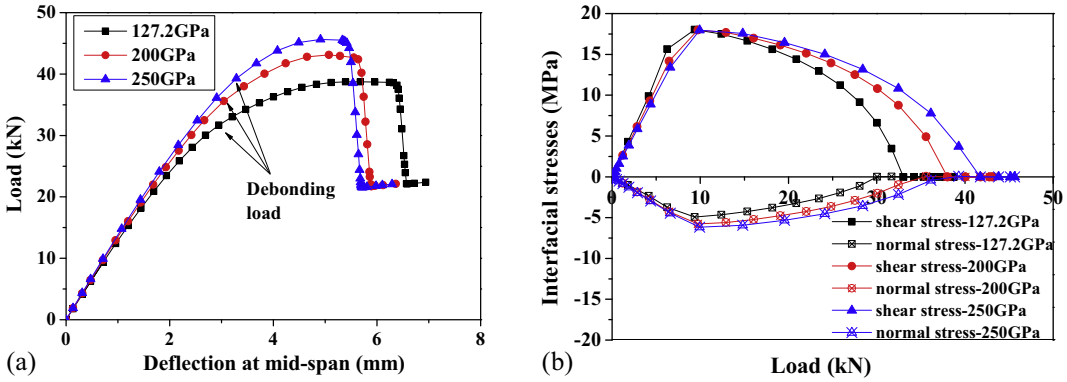

Fig. 12. Strengthened beam with different CFRP elastic moduli: (a) Load-deflection curves; (b) Interfacial stress-load relationship.

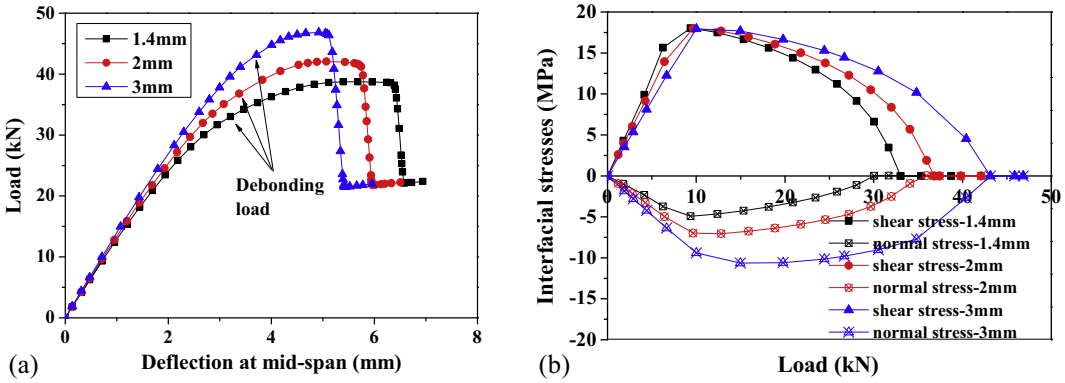

Fig. 13. Strengthened beam with different CFRP thicknesses: (a) Load-deflection curves; (b) Interfacial stress-load relationship.

ferent elastic moduli. As shown in Fig. 12 (b), for CFRP with elastic moduli of 127.2 GPa, 200 GPa and 250 GPa, the shear and normal stresses reached the maximum values at loads of 9.36 kN, 9.72 kN and 9.93 kN, respectively. There was no obvious difference observed in the ascending stage, which means the elastic modulus has an insignificant effect on adhesive layer degradation. In addition, for each case, when the load increased to 33.02 kN, 38 kN and 41.74 kN, the shear stress and normal stress decreased to zero, indicating the initiation of debonding. Therefore, the higher the CFRP elastic modulus is, the higher the interfacial stress near the notch when the adhesive layer is softening and the lower the rate of degradation. Meanwhile, the debonding load and ultimate load of the strengthened steel beams can be improved at higher elastic moduli. It is worth noting that a different trend was observed for the plate-end debonding failure. The higher the elastic modulus of the CFRP plate was, the lower the debonding load [12].

6.3. CFRP thickness

The CFRP thickness can affect the strength of strengthened steel beams [13]. To enhance the understanding of the effect of the CFRP thickness on the strengthening of notched steel beams, in consideration of previous experimental studies and common engineering applications, three CFRP thicknesses (1.4 mm, 2 mm and 3 mm) were selected for the FEM analysis. The load-deflection results are shown in Fig. 13(a). The thicker the CFRP plate is, the higher the observed ultimate load. However, as the ultimate load increases, the deflection decreases. When the CFRP thickness increased from 1.4 mm to 2 mm and 3 mm, the debonding load increased 11.5% and 30.7%, the ultimate load increased 8.7% and 21%, whereas the deflection decreased 6.2% and 14.2%, respectively. Therefore, the bearing capacity of strengthened steel beams can be effectively improved by increasing the CFRP plate thickness, but the sacrifice of ductility should be noted.

Fig. 13(b) shows the interfacial stress and load relationship. When the shear and normal stresses reached their maximum values, the loads of the strengthened steel beams were 9.36 kN, 9.64 kN and 14.96 kN. Then, the shear and normal stresses decreased to zero (CFRP thickness 1.4 mm, 2 mm and 3 mm) when the loads were 33.02 kN, 36.82 kN and 43.15 kN. Clearly, the effect of the thickness is similar to that of the CFRP elastic modulus. Using a thicker CFRP plate could also be an effective way to improve the debonding and ultimate loads. The results could be beneficial reference for the design of CFRP strengthening. However, as discussed in the above section, the conclusion may only be valid for strengthened deficient steel beams. For strengthened sound steel beams, plate-end debonding can occur, and the increase of CFRP thickness has a negative effect on the debonding strength [12].

7. Conclusions

In this paper, the mixed-mode cohesive law was applied to simulate notched steel beams strengthened by CFRP plates, and authors' theoretical and experimental results were compared for model verification. As discussed, the following conclusions can be made.

(1) The mixed-mode cohesive law was validated by the experimental results as an effective model for simulating the mechanical behaviour of notched steel beams strengthened by CFRP plates. Compared with the average debonding and

ultimate loads from test and FEM results, the deviations are about 6.0% and 5.4%, respectively. The accuracy of the model is also demonstrated by the load-deflection curves and the strain distributions at the debonding load and ultimate load.

(2) The debonding process of notched steel beams strengthened with CFRP plates can be accurately simulated by the numerical model. How the longitudinal shear stress and normal stress change with increasing load is clear from the simulated results. The simulation tool is important for the development of debonding prevention measures and improvement of the bearing capacity.

(3) The simulated results agree with the theoretical results for specimens in the elastic stage. However, the difference becomes obvious in the plastic stage, which implies that the results from the theoretical calculation were overestimated. For better accuracy and safety, in engineering applications, it is necessary to predict the debonding and ultimate loads of specimens using numerical models.

(4) The effects of the notch depth, CFRP elastic modulus and CFRP thickness were assessed through parametric analysis. The debonding load and ultimate load of the strengthened steel beams decreased with the notch depth substantially. Moreover, the bearing capacity increased with the elastic modulus and thickness of the CFRP plates, while the ductility decreased, resulting in premature debonding failure. When the CFRP elastic moduli increased from 127.2 GPa to 200 GPa and 250 GPa, the debonding load increased 15.1% and 26.4%, the ultimate load increased 11.4% and 17.8%, respectively. In addition, when the CFRP thickness increased from 1.4 mm to 2 mm and 3 mm, the debonding load increased 11.5% and 30.7%, the ultimate load increased 8.7% and 21%, respectively. The results are only valid for strengthened deficient steel beams that are subject to intermediate debonding failure since increases in the CFRP elastic modulus and thickness have negative effects in cases of plate-end debonding failure.

Acknowledgements

This work is supported by the National Natural Science Foundation of China through Grants (Project No. 51778151, 51708133, 51278131), the Department of Education of Guangdong Province, China (Project No. 2016KZDXM051), and by China Postdoctoral Science Foundation (Project No. 2017M622633).

References

[1] T. Andersson, U. Stigh, The stress–elongation relation for an adhesive layer loaded in peel using equilibrium of energetic forces, Int. J. Solids Struct. 41 (2) (2004) 413–434.
[2] M. Bocciarelli, P. Colombi, G. Fava, C. Poggi, Interaction of interface delamination and plasticity in tensile steel members reinforced by CFRP plates, Int. J. Fract. 146 (1–2) (2007) 79–92.
[3] M. Bocciarelli, P. Colombi, G. Fava, C. Poggi, Prediction of debonding strength of tensile steel/CFRP joints using fracture mechanics and stress based criteria, Eng. Fract. Mech. 76 (2) (2009) 299–313.
[4] M. Bocciarelli, P. Colombi, On the elasto-plastic behavior of continuous steel beams reinforced by bonded CFRP lamina, Eng. Struct. 49 (2013) 756–766.
[5] P.P. Camanho, C.G. Davila, Mixed-mode decohesion finite elements for the simulation of delamination in composite materials, NASA 6 (2002) 1–37.
[6] P.P. Camanho, C.G. Davila, M.F. De Moura, Numerical simulation of mixed-mode progressive delamination in composite materials, J. Compos. Mater. 37 (16) (2003) 1415–1438.
[7] R. Campilho, M.D. Moura, J. Domingues, Using a cohesive damage model to predict the tensile behaviour of CFRP single-strap repairs, Int. J. Solids Struct. 45 (5) (2008) 1497–1512.
[8] J. Chen, J. Teng, Anchorage strength models for FRP and steel plates bonded to concrete, J. Struct. Eng. 127 (7) (2001) 784–791.
[9] P. Colombi, Reinforcement delamination of metallic beams strengthened by FRP strips: fracture mechanics based approach, Eng. Fract. Mech. 73 (14) (2006) 1980–1995.
[10] P. Colombi, C. Poggi, An experimental, analytical and numerical study of the static behavior of steel beams reinforced by pultruded CFRP strips, Compos. B Eng. 37 (1) (2006) 64–73.
[11] J. Dai, T. Ueda, Y. Sato, Development of the nonlinear bond stress–slip model of fiber reinforced plastics sheet–concrete interfaces with a simple method, J. Compos. Constr. 9 (1) (2005) 52–62.
[12] J. Deng, M.M. Lee, S.S. Moy, Stress analysis of steel beams reinforced with a bonded CFRP plate, Compos. Struct. 65 (2) (2004) 205–215.
[13] J. Deng, M.M.K. Lee, Behaviour under static loading of metallic beams reinforced with a bonded CFRP plate, Compos. Struct. 78 (2) (2007) 232–242.
[14] J. Deng, M.M.K. Lee, Adhesive bonding in steel beams strengthened with CFRP, Struct. Build. 162 (4) (2009) 241–249.
[15] J. Deng, Y. Jia, H. Zheng, Theoretical and experimental study on notched steel beams strengthened with CFRP plate, Compos. Struct. 136 (2016) 450–459.
[16] A. Fam, MacDougall, A. Shaat, Upgrading steel-concrete composite girders and repair of damaged steel beams using bonded CFRP laminates, Thin-Walled Struct. 47 (10) (2009) 1122–1135.
[17] Fawzi, X.L. Zhao, Al-Mahaidi, S. Rizkalla, Bond characteristics between CFRP and steel plates in double strap joints, Int. J. Adv. Steel Constr. 1 (2) (2005) 17–28.
[18] S. Fawzia, R. Al-Mahaidi, X.L. Zhao, Experimental and finite element analysis of a double strap joint between steel plates and normal modulus CFRP, Compos. Struct. 75 (1–4) (2006) 156–162.
[19] S. Fawzia, X.-L. Zhao, R. Al-Mahaidi, Bond–slip models for double strap joints strengthened by CFRP, Compos. Struct. 92 (9) (2010) 2137–2145.
[20] D. Fernando, T. Yu, J.G. Teng, Behavior of CFRP laminates bonded to a steel substrate using a ductile adhesive, J. Compos. Constr. 18 (2) (2013) 04013040.
[21] B. Fu, J.G. Teng, J.F. Chen, G.M. Chen, Y.C. Guo, Concrete cover separation in FRP-plated RC beams: mitigation using FRP U-jackets, J. Compos. Constr. 21 (2) (2017) 1–13.
[22] E. Ghafoori, M. Motavalli, Normal, high and ultra-high modulus carbon fiber-reinforced polymer laminates for bonded and un-bonded strengthening of steel beams, Mater. Des. 67 (2015) 232–243.
[23] R. Haghani, Analysis of adhesive joints used to bond FRP laminates to steel members – a numerical and experimental study, Constr. Build. Mater. 24 (11) (2010) 2243–2251.
[24] R. Haghani, M. Al-Emrani, R. Kliger, Interfacial stress analysis of geometrically modified adhesive joints in steel beams strengthened with FRP laminates, Constr. Build. Mater. 23 (3) (2009) 1413–1422.
[25] A. Hmidan, Y.J. Kim, S. Yazdani, CFRP repair of steel beams with various initial crack configurations, J. Compos. Constr. 15 (6) (2011) 952–962.
[26] L.C. Hollaway, J. Cadei, Progress in the technique of upgrading metallic structures with advanced polymer composites, Prog. Struct. Mat. Eng. 4 (2) (2002) 131–148.
[27] S.C. Jones, S.A. Civjan, Application of fiber reinforced polymer overlays to extend steel fatigue life, J. Compos. Constr. 7 (4) (2003) 331–338.
[28] A. Lenwari, T. Thepchatri, P. Albrecht, Debonding strength of steel beams strengthened with CFRP plates, J. Compos. Constr. 10 (1) (2006) 69–78.
[29] A. Lenwari, T. Thepchatri, P. Santisukpotha, A fracture-based criterion for debonding strength of adhesive-bonded double-strap steel joints, Eng. J. 16 (1) (2012) 17–26.
[30] D. Linghoff, M. Al-Emrani, R. Kliger, Performance of steel beams strengthened with CFRP laminate–Part 1: laboratory tests, Compos. B Eng. 41 (7) (2010) 509–515.
[31] D. Linghoff, M. Al-Emrani, Performance of steel beams strengthened with CFRP laminate–Part 2: FE analyses, Compos. B Eng. 41 (7) (2010) 516–522.
[32] D.J. Oehlers, FRP plates adhesively bonded to reinforced concrete beams: generic debonding mechanisms, Adv. Struct. Eng. 9 (6) (2006) 737–750.
[33] S. Rizkalla, M. Dawood, D. Schnerch, Development of a carbon fiber reinforced polymer system for strengthening steel structures, Compos. A Appl. Sci. Manuf. 39 (2) (2008) 388–397.
[34] R. Sen, L. Liby, G. Mullins, Strengthening steel bridge sections using CFRP laminates, Compos. B Eng. 32 (4) (2001) 309–322.
[35] D. Schnerch, S. Rizkalla, Flexural strengthening of steel bridges with high modulus CFRP strips, J. Bridge Eng. 13 (2) (2008) 192–201.
[36] Schnerch, Dawood, Rizkalla, Sumner, Stanford, Bond behavior of CFRP strengthened steel structures, Adv. Struct. Eng. 9 (6) (2009) 805–817.
[37] T. Stratford, J. Cadei, Elastic analysis of adhesion stresses for the design of a strengthening plate bonded to a beam, Constr. Build. Mater. 20 (1–2) (2006) 34–45.
[38] A. Shaat, A. Fam, Repair of cracked steel girders connected to concrete slabs using carbon fiber reinforced polymer sheets, J. Compos. Constr. 12 (6) (2008) 650–659.
[39] M. Tavakkolizadeh, H. Saadatmanesh, Fatigue strength of steel girders strengthened with carbon fiber reinforced polymer patch, J. Struct. Eng. 129 (2) (2003) 186–196.
[40] J. Teng, T. Yu, D. Fernando, Strengthening of steel structures with fiber-reinforced polymer composites, J. Constr. Steel Res. 78 (2012) 131–143.
[41] J.G. Teng, D. Fernando, T. Yu, Finite element modelling of debonding failures in steel beams flexurally strengthened with CFRP laminates, Eng. Struct. 86 (2015) 213–224.

[42] B. Wang, Y. Bai, X. Hu, P. Lu, Enhanced epoxy adhesion between steel plates by surface treatment and CNT/short-fibre reinforcement, Compos. Sci. Technol. 127 (2016) 149–157.
[43] Y. Wang, J. Li, J. Deng, W. Xie, Y. Zheng, Numerical study on notched steel plate with center hole strengthened by CFRP, J. Adhes. Sci. Technol. (2017) 1–15.
[44] Y. Wang, C. Zhou, Bond characteristics of CFRP/steel interface end-anchored with G-shaped clamps, Polym. Polym. Compos. 25 (9) (2017) 661–667.
[45] C. Wu, X. Zhao, W. Hui Duan, R. Al-Mahaidi, Bond characteristics between ultra high modulus CFRP laminates and steel, Thin-Walled Struct. 51 (2012) 147–157.
[46] S.H. Xia, J.G. Teng, Behaviour of FRP-to-steel bonded joints, Proc., International Symposium on Bond Behaviour of FRP in Structures, 2005, 411–418.
[47] J.Q. Yang, S.T. Smith, P. Feng, Effect of FRP-to-steel bonded joint configuration on interfacial stresses: Finite element investigation, Thin-Walled Struct. 62 (2013) 215–228.
[48] M. Youssef, Analytical prediction of the linear and nonlinear behaviour of steel beams rehabilitated using FRP sheets, Eng. Struct. 28 (6) (2006) 903–911.
[49] Q.Q. Yu, Y.F. Wu, Fatigue strengthening of cracked steel beams with different configurations and materials, J. Compos. Constr. 04016093 (2016) 1–12.
[50] T. Yu, D. Fernando, J.G. Teng, X.L. Zhao, Experimental study on CFRP-to-steel bonded interfaces, Compos. B Eng. 43 (5) (2012) 2279–2289.
[51] Y. Yu, S. Chiew, C. Lee, Bond failure of steel beams strengthened with FRP laminates–Part 2: Verification, Compos. B Eng. 42 (5) (2011) 1122–1134.
[52] X.-L. Zhao, L. Zhang, State-of-the-art review on FRP strengthened steel structures, Eng. Struct. 29 (8) (2007) 1808–1823.
[53] D. Zhang, S. Shen, Y. Zhao, W. Jin, T. Ueda, Cracking behavior of CFRP laminate-strengthened RC beams with premechanical and postmechanical environmental damage, J. Compos. Constr. 19 (4) (2014) 04014066.
[54] D. Zhang, Y. Zhao, T. Ueda, X. Li, Q. Xu, CFRP strengthened RC beams with pre-strengthening non-uniform reinforcement corrosion subjected to post-strengthening wetting/drying cycles, Eng. Struct. 127 (2016) 331–343.
[55] D. Zhang, H. Shi, J. Zhu, M. Su, W. Jin, Cover separation of CFRP strengthened beam-type cantilevers with steel bolt anchorage, Eng. Struct. 156 (2018) 224–234.
[56] H. Zhou, T.L. Attard, Y. Wang, J.-A. Wang, F. Ren, Rehabilitation of notch damaged steel beams using a carbon fiber reinforced hybrid polymeric-matrix composite, Compos. Struct. 106 (2013) 690–702.